SAND2015-10521C

Fluid-Structure Interactions using Controlled Disturbances on a Slender Cone at Mach 8

Katya M. Casper*, Steven J. Beresh†, John F. Henfling‡, Russell W. Spillers§, and Patrick Hunter¶
Sandia National Laboratories, Albuquerque, NM 87185

Fluid-structure interactions were studied on a 7° half-angle cone in the Sandia Hypersonic Wind Tunnel at Mach 8 over a range of freestream Reynolds numbers between 3.3 and $14.5 \times 10^6/m$. A thin panel with tunable structural natural frequencies was integrated into the cone and exposed to naturally developing boundary layers. An elevated panel response was measured during boundary-layer transition, and lower vibrations were measured under a turbulent boundary layer. The elevated transitional vibrations were measured at frequencies corresponding to the turbulent burst rate, though further investigation of this relationship is warranted.

Controlled perturbations from an electrical discharge were then introduced into the boundary layer at varying frequencies corresponding to the structural natural frequencies of the panel. The perturbations were not strong enough to drive a panel response exceeding that due to natural transition at the structural natural frequencies. Instead at high repetition rates, the perturber modified the boundary layer by increasing the boundary-layer intermittency and simultaneously decreasing the turbulent burst rate on the cone. As a result, the controlled perturbation generated an elevated transitional panel vibration response at a lower Re than the corresponding natural transition case.

Nomenclature

δ	boundary-layer thickness (mm)	t	time (s)
ϕ	cone azimuthal angle (°)	T_0	tunnel stagnation temperature (K)
f	frequency (kHz)	U_e	boundary-layer edge velocity (m/s)
M	freestream Mach number	x	axial model coordinate measured from nose (mm)
P_0	tunnel stagnation pressure (kPa)	y	spanwise model coordinate measured from $\phi = 0°$,
p'	pressure fluctuation, $p - p_e$ (Pa)		clockwise along the cone circumference,
p_e	boundary-layer edge pressure (Pa)		looking upstream (mm)
q_e	dynamic pressure at boundary-layer edge (Pa)	z	surface normal model coordinate (mm)
Re	freestream unit Reynolds number (1/m)		

I. Introduction

Hypersonic reentry vehicles are subjected to high levels of fluctuating pressures. These intense fluctuations can cause vibration of internal components and lead to structural problems. There is a need to predict the magnitude, frequency content, location, and spatial extent of the pressure fluctuations to better design hypersonic flight vehicles. Previous work has focused on the fluid dynamics of the problem and better understanding the generation of transitional pressure fluctuations.[1–3]

*Senior Member of the Technical Staff, Engineering Sciences Center, Member AIAA, kmcaspe@sandia.gov, (505) 844-1574
†Distinguished Member of the Technical Staff, Engineering Sciences Center, Associate Fellow AIAA
‡Distinguished Technologist, Engineering Sciences Center, Member AIAA
§Principal Technologist, Engineering Sciences Center
¶Principal Technologist, Engineering Sciences Center

Sandia National Laboratories is a multi-program laboratory managed and operated by Sandia Corporation, a wholly owned subsidiary of Lockheed Martin Corporation, for the U.S. Department of Energy's National Nuclear Security Administration under contract DE-AC04-94AL85000.

The interaction of the fluctuations with the vehicle structure also needs to be better understood, but there is very limited experimental work studying such high-speed fluid-structure interactions. A significant portion of the existing experimental literature has focused on the panel response to unsteady shock-boundary layer interactions.[4–6] Some complementary computational work has also been done exploring this interaction.[7,8] In the present case, however, the application is the response of a thin panel to excitation by boundary-layer pressure fluctuations. There has been some work studying the response to supersonic turbulent boundary layers,[9–11] but little focusing on transitional boundary layers. One low-speed study (M = 0.3–0.5) did address transitional boundary layers and was able to measure the increased pressure fluctuations generated by the intermittent boundary layer.[12] However, the increased pressure fluctuations were not directly tied to any change in the panel response.

The present work seeks to develop a dataset to study fluid-structure interactions to hypersonic transitional and turbulent boundary layers. A thin panel was integrated into a 7° half-angle cone at zero angle of attack. The panel was designed to have varying structural natural frequencies that could be tuned to match the flow excitation frequencies by varying the panel material or the material of attached weights. The cone and panel were then tested in the Sandia National Laboratories Hypersonic Wind Tunnel (HWT) at Mach 8 over a range of freestream Re between 3.3 and $14.5 \times 10^6/m$. The panel response to naturally developed laminar, transitional, and turbulent boundary layers was characterized. The natural transition case, however, provided an uncontrolled environment that could not be tuned to the structural natural frequencies of the panel. In order to do this, a controlled perturber was developed and used to introduce flow disturbances into the boundary layer at input frequencies up to 10 kHz. The response of the panel to controlled perturbations was then studied.

II. Experimental Setup

II.A. Sandia Hypersonic Wind Tunnel

The Sandia Hypersonic Wind Tunnel (HWT) is a conventional blowdown-to-vacuum facility. Interchangeable nozzle and heater sections allow the tunnel to be run at Mach 5, 8 or 14. Experiments were only conducted at Mach 8 for the present work. Run times were typically 40 s. HWT-8 uses 689 MPa nitrogen supplied from a bottle farm. It has a P_0 range of 1720–6890 kPa, T_0 range of 500–890 K, and Re can be varied from $3.3–20 \times 10^6/m$. Noise levels vary from 3–5%.[13] Freestream conditions in this tunnel are computed using the Beattie-Bridgeman model to account for real-gas effects. At the low freestream temperatures in these tunnels, a linear viscosity law is used. Edge conditions used for normalization of the data were computed using a Taylor-Maccoll solution for flow over the cone.

II.B. Model and Instrumentation

A 0.517-m-long 7° half-angle stainless-steel cone was used for the present work (Fig. 1). This model is similar to that used in previous experimental campaigns that were focused on better understanding transitional pressure fluctuations.[3] Both a sharp (radius less than 0.05 mm) and a 1.5 mm radius blunt nose were used. The cone was designed to accept a thin panel at the aft end of the cone. Two panels were built: one of stainless steel and the other of carbon-composite material. The center of each panel had a mounting point to accept different weights made of either aluminum, steel, or tungsten. Each of these modifications varied the structural natural frequencies of the panel.

The panel itself was approximately 63.5 mm long, and encompassed 80 degrees of the cone circumference. The panel thickness was 1 mm, but there was a 5-mm thick and 5-mm wide frame around the outside edge of the panel to allow mounting into the cone and to provide a better 'fixed' boundary condition. Fig. 2 show external and internal views of the carbon-composite panel, without an attached weight. The panel was glued into the model with RTV around the frame. Three flathead screws along the left and right sides and the aft end of the panel helped secure it to the model. The heads of the screws were covered with plaster that was sanded flush with the cone surface to eliminate any roughness that might introduce disturbances into the flow. Also, a mounting screw was not used on the center of the panel leading edge to again ensure that disturbances were not introduced into the boundary layer by any residual roughness.

Two types of accelerometers were used to measure the panel response. A PCB356A03 miniature triaxial accelerometer, $G1$, was attached to the weight on the inside of the panel. When a weight was not installed, the accelerometer was instead glued to the weight mounting point. This sensor has a flat frequency response

(±5%) to about 5 kHz along the x-axis and to 8 kHz along the y and z axes. On the panel itself, three uniaxial PCB352A73 sensors were used to measure the wall-normal panel acceleration along the z axis, though only one, $G5$, is discussed here. These sensors have a flat frequency response to 10 (±5%) or to 25 kHz (±10%). The location of the accelerometers is specified in Table 2. Fig. 3 shows an internal view of the cone with accelerometers mounted to the inside of the panel for a structural hammer test.

The fluid forcing of the panel was characterized by PCB132 sensors upstream and downstream of the panel. These sensors are very high frequency piezoelectric time-of-arrival sensors that can be used to measure pressure fluctuations between 11 kHz and 1 MHz. This high frequency response allows a study of instability breakdown to transition on the cone (typically near 200 kHz) and is a useful indicator of transition on the model. Also, the sensors have adequate frequency response to resolve the short duration of turbulent spots on the cone (on the order of 0.01 ms[14]). Although these sensors cannot characterize the pressure fluctuations on the cone below 10 kHz, they allow unsteady boundary-layer phenomena to be characterized and boundary-layer statistics to be computed with high temporal resolution. More information about the use of these sensors to characterize the pressure fluctuations can be found in Refs. 14 and 3.

The PCB132 sensor signals all run through a PCB 482A22 signal conditioner that provides constant-current excitation to the built-in sensor amplifier. It also decouples the AC signal from the DC bias voltage. The output from the signal conditioner is fed through a Krohn-Hite Model 3944 Filter with a 1.25 MHz low-pass anti-aliasing Bessel filter. This filter has four poles and offers 24 dB of attenuation per octave. The sampling frequency for the PCB132 signals was 2.5 MHz. Pressure sensor data was acquired using a National Instruments PXI-1042 chassis with 14-bit PXI-6133 modules (10 MHz bandwidth). The acceleration signals were sent to a data acquisition system (NI 9232), where they passed through an anti-aliasing filter prior to being digitized at a sampling rate of 102.4 kHz. Triggering of the perturber, schlieren system, and data acquisition was controlled by Stanford Research Systems DG645 Digital Delay Generators.

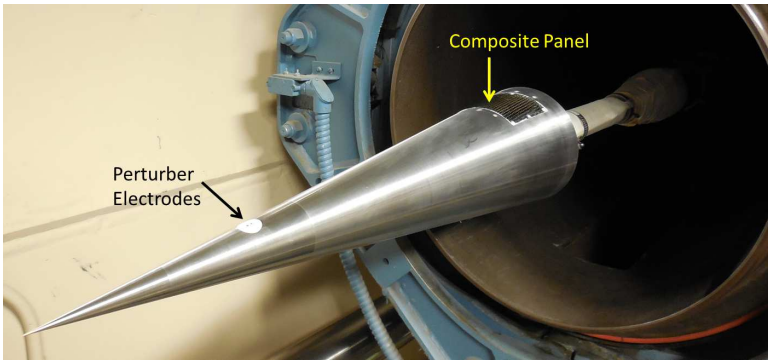

Figure 1. Wind-tunnel model with integrated panel installed in Sandia Hypersonic Wind Tunnel.

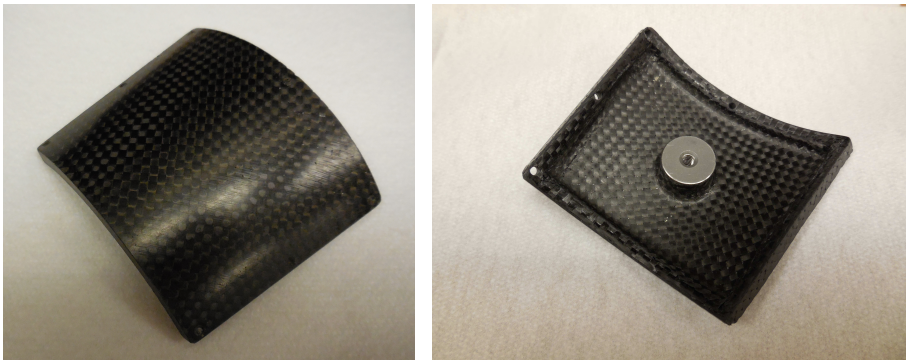

(a) (b)

Figure 2. Carbon-composite panel (a) External view; (b) Internal view.

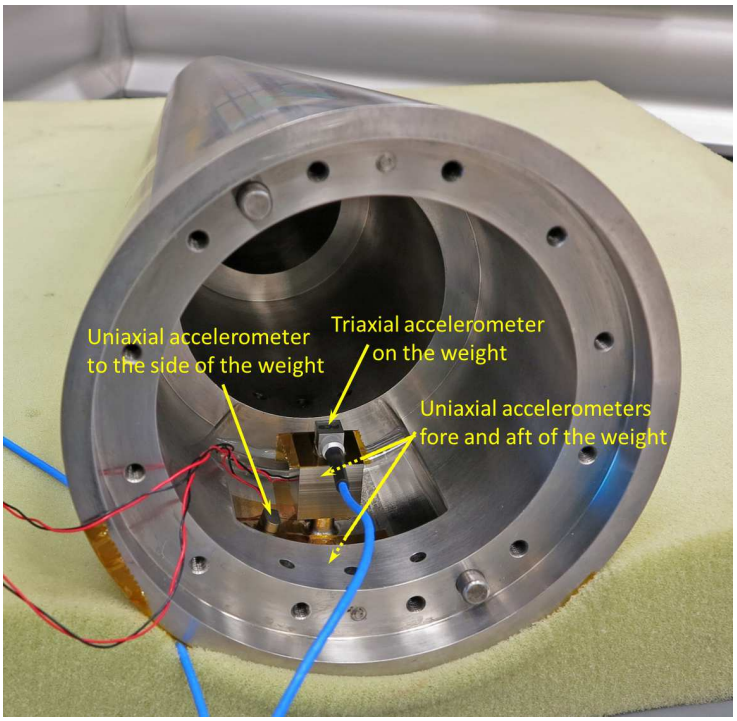

Figure 3. Internal view of cone showing the thin stainless steel panel, attached weight, and accelerometers.

Table 1. Location of pressure sensors on the thin-panel cone.

Location	x (mm)	$\phi(^\circ)$	y (mm)
P1	421.5	-20	-18.1
P2	421.5	0	0.0
P3	421.5	20	18.1
P4	497.2	-20	-21.3
P5	497.2	0	0.0
P6	497.2	20	21.3

Table 2. Location of accelerometers on the thin-panel cone.

Location	Description	x (mm)	$\phi(^\circ)$	y (mm)
G1	Triaxial, On mass center	459.3	0	0.0
G5	Uniaxial, Downstream of mass	475.1	0	0.0

II.C. Thin-Panel Cone Structural Hammer Test

A calibrated hammer test was conducted to identify the structural natural frequencies of the model and panels up to 10 kHz. The hammer test provided the frequency response functions (FRF) of the different structures as well as their mode shapes. A typical example of an FRF is shown in Fig. 4 for a carbon composite panel with different attached weights. This FRF shows a ratio of the calibrated force input over the acceleration response of the panel. The dominant mode shows a frequency shift as the attached weight is varied. This tuning allows the structural natural frequencies of the panel to be matched to the flow excitation frequencies. Key structural mode frequencies and mode shape descriptions for some panel configurations are given in Table 3. Results of other configurations are not shown as they were not tested in the Mach 8 tunnel.

Mode shapes corresponding to the different structural natural modes of the panel were also obtained from the acceleration measurements. Some of the typical mode shapes are shown in Fig. 5 with an exaggerated scale to make the shapes clear. The two lobe panel modes P_y and P_x correspond to a sine wave mode shape aligned with panel in the spanwise and axial directions, respectively. These mode shapes have maxima away from the panel center. The 3-lobe panel mode P_z has a large displacement at the center of the panel. Two other off-axis lobes occur in the spanwise direction, but have a much smaller displacement than the panel center. Yet another mode, P_f, corresponds to the displacement of the front edge of the panel, though this mode only showed up for the carbon-composite panel. The front edge does not have a screw holding the frame in place since it was thought that this could disturb the boundary layer. As a result, there is a larger displacement of the panel front, with respect to the other panel edges. In addition to the panel modes, spanwise (M_y) and axial (M_x) rocking modes of attached masses were measured. Many other mode frequencies and complex mode shapes were identified by the hammer test, but are not discussed further.

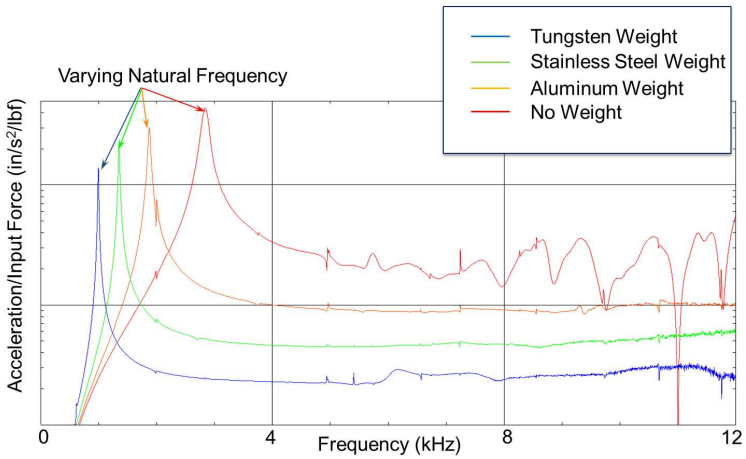

Figure 4. Typical Frequency Response Function, carbon composite panel.

Table 3. Modes of thin-panel cone with the carbon-composite and stainless steel panels.

Weight:	**Tungsten**		**None**	
Composite Panel Modes	**Frequency (Hz)**	**Damping %**	**Frequency (Hz)**	**Damping %**
2 lobe panel mode, lobes along Y (P_y)	394	0.64	2099	2.57
2 lobe panel mode, lobes along X (P_x)	604	0.79	3381	4.96
3 lobe panel mode, mostly motion in center lobe (P_z)	990	0.7	2831	2.44
Front edge of panel (P_f)	6117	2.62	7539	3.71
Stainless Panel Modes				
2 lobe panel mode, lobes along Y (P_y)	3002	0.49	-	-
2 lobe panel mode, lobes along X (P_x)	3458	0.52	10316	0.83
3 lobe panel mode, mostly motion in center lobe (P_z)	1637	0.19	4960	0.16
Mass Modes				
Mass Rocking Horizontally (Y) (M_y)	419	0.67	-	-
Mass Rocking Axially (X) (M_x)	439	0.55	-	-

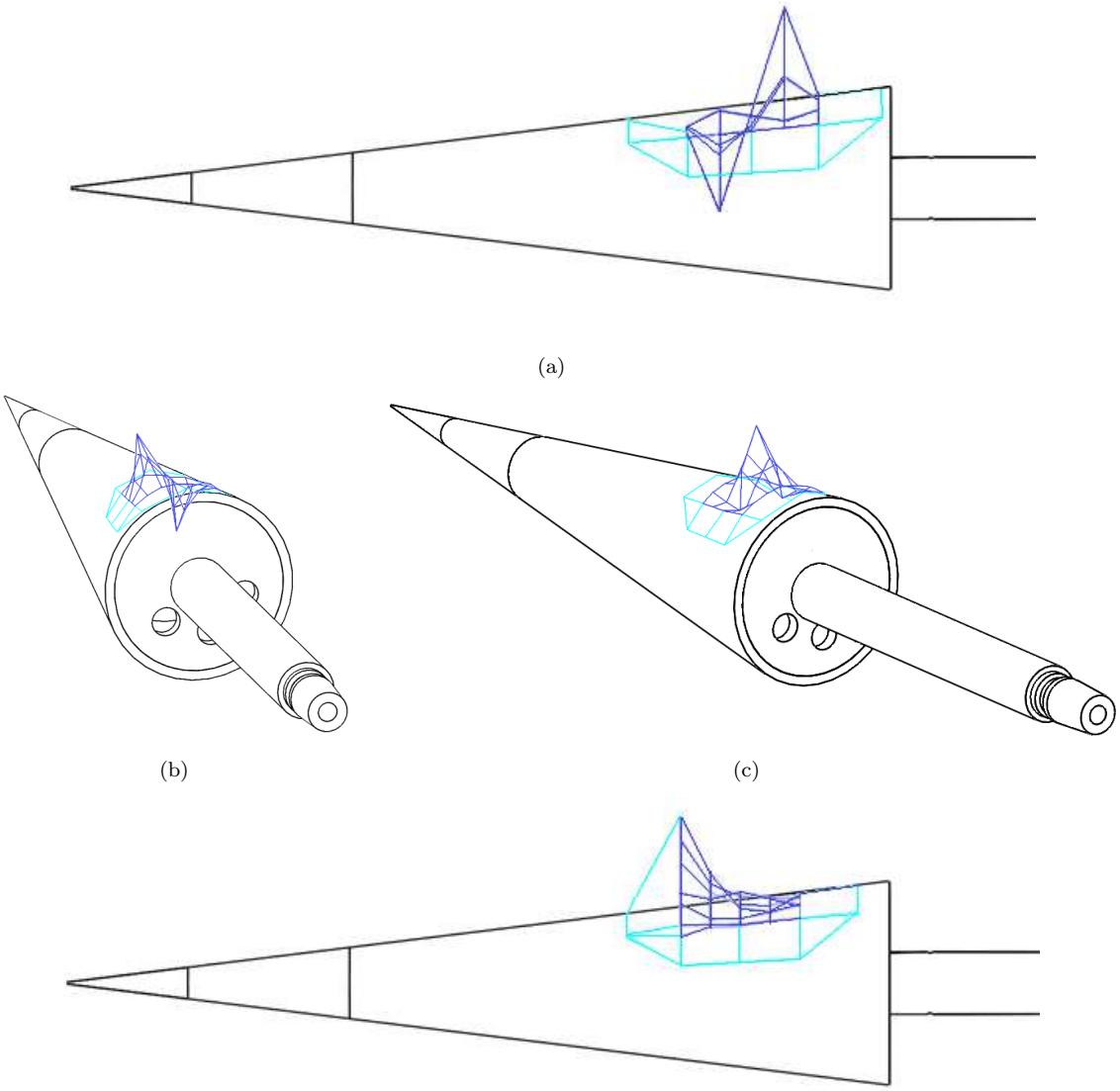

(a)

(b)

(c)

(d)

Figure 5. Typical mode shapes of panel (a) Two-lobe panel mode along X, P_x; (b) Two-lobe panel mode along Y, P_y; (c) 3-lobe panel mode, P_z; (d) Front panel edge mode, P_f.

II.D. Glow Perturber

Disturbances were introduced into the cone boundary layer using a controlled flow perturber upstream of the panel at x = 0.137 m. The perturber is similar to that previously used at Mach 6 in the Boeing/AFOSR Mach-6 Quiet Tunnel at Purdue,[2] however, the present experiments use improved electronics for more repeatability and the ability to create perturbations at faster repetition rates. New perturber electronics were designed and built by High Voltage Connection. The electronics incorporate a Behlke high-voltage transistor and an accompanying driving circuit. The voltage output is variable between 0 and 2 kV. A current limiter allows the discharge current to be controlled over a wide range. Together, the voltage and current adjustably allows the discharge to be varied between a glow or spark discharge.[15] The quoted pulse duration is between 1 and 100 μs at repetition rates of up to 1 kHz.

In practice, the perturber was operated with a duration of 4 μs. This is because the discharge initiated by the perturber only lasts 4 μs, despite the control input which might call for a longer duration. Fig. 6 shows an example of this. Current transducer measurements of the discharge are shown for varying control lengths of Δt. The discharge is initiated at time t = 0 and is characterized by a high current near 9A. The discharge ends after approximately 4 μs when the current returns to zero. This always occurs near 4 μs, regardless of the input control. There is then a second, smaller, discharge when the control input is turned off at Δt. As a result, the input control was maintained at 4 μs to coincide with the natural discharge length. Typically, the electronics were operated without a current limiter and with the maximum voltage output of 2 kV in order to generate a spark discharge. This was because the Mach 8 flow proved difficult to perturb, and the maximum flow perturbation possible was desired.

Repetition rates of 250 Hz to 10 kHz were demonstrated, though the repeatability of the perturber decreased at higher repetition rates. For rates near 1 kHz, repeatability and reliability of the discharge was good. There was little jitter in the firing time of the perturber which remained below 0.1 μs. As the repetition rate was increased to 10 kHz, the repeatability and reliability of firing gradually worsened. Jitter on the order of 0.5 μs was seen, and sometimes a discharge was not initiated. At repetition rates above 10 kHz, the perturber electronics could not recover fast enough and subsequent perturbations were smaller in amplitude.

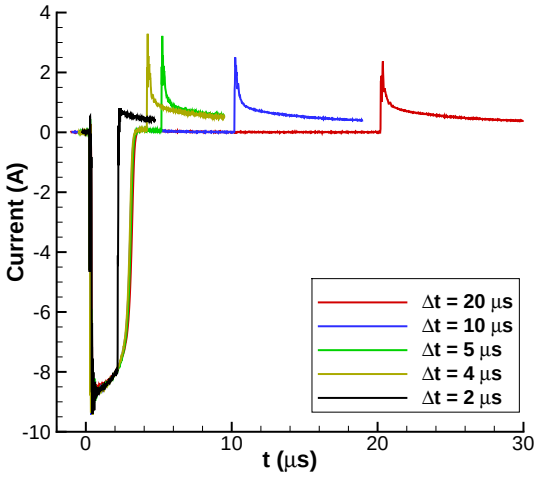

Figure 6. Perturber pulse duration, current measurements.

III. Results

III.A. Controlled Perturbations over a Slender Cone

Before looking at the fluid-structure interaction results, it is useful to consider the natural pressure fluctuations on the cone at varying Reynolds numbers, and the effect of the glow perturber at these same conditions. Results are shown here for a 1.5 mm radius nosetip which delays natural transition on the cone, in comparison to a sharp nosetip.[13] This delay was desired in order to minimize natural disturbance growth and

allow the study of mostly the controlled disturbances. For characterizing the effect of the perturber on the boundary layer, a similar cone with dense arrays of pressure sensors was used for some of the measurements. This cone and its sensor locations are described in detail in Ref. 3.

Figs. 7(a) – 7(c) show ensemble-averaged pressure traces of 400 samples from sensors in an axial insert at varying Re. The control signal to the perturber was used for the timing of the ensemble average for this data set. The ensemble averages clearly show the controlled disturbances between 0.2 and 0.3 ms after the input perturbation. At the lowest Re of $4.1 \times 10^6/m$, a small wave packet is observed as it convects and grows downstream. Unfortunately, the perturber does not create a large enough disturbance to induce turbulent spots at this Re. At a higher Re of $8.4 \times 10^6/m$, the ensemble averages show a large wave packet at x = 0.355 m that gradually begins to break down by x = 0.396 m. However, it is also clear that natural second-mode waves are also developing. These natural waves show up as periodic disturbances in the ensemble averages at this Re. At the highest Re of $14.5 \times 10^6/m$, a turbulent spot is observed growing and convecting downstream. This spot shows up as a region of higher average pressure since the random turbulent fluctuations are smoothed out by the ensemble averaging. Outside of the controlled spot, large natural waves are again observed in the ensemble average. The relative amplitude of the controlled versus natural disturbances can be more clearly seen by looking at a typical individual sample at $Re = 14.5 \times 10^6/m$ that has not been ensemble averaged (Fig. 7(d)). Without the ensemble averaging, the high-frequency turbulent fluctuations within the spots can be seen, however, the turbulent spot is occurring within the growth of natural second-mode waves with similar fluctuation amplitudes. It therefore appears that the perturber can initiate the breakdown of second-mode waves into turbulent spots at high Re (where natural waves and spots are also occurring), but the perturber is not powerful enough to create turbulent spots at lower Re where the growth of natural disturbances is limited.

Because the perturber does not dominate the transition process, it is useful to characterize the boundary-layer state with and without the perturber firing. The turbulent burst rate and turbulent intermittency over the panel were computed from PCB132 pressure measurements on the cone as described in Ref. 14. These high frequency pressure measurements clearly show the boundary layer state as it fluctuates between instability waves and turbulence. This allows boundary-layer transition statistics to be computed. Low frequency pressure measurements, on the other hand, cannot distinguish instability waves from turbulence, and therefore do not give a clear picture of the unsteady characteristics of the boundary layer.

Fig. 8(a) shows the burst rate and intermittency over a range of freestream Re at x = 0.422 m, with and without the perturber firing at 7.9 kHz, for a sharp nosetip. As can be seen, the intermittency of the boundary-layer increases, and the turbulent burst rate decreases with the perturber firing at this high repetition rate. This is because the perturber creates more regions of turbulent flow, which creates less unsteady switching between laminar and turbulent regions, and more overall turbulence. It should be noted that the measured burst rate is not 7.9 bursts/ms. This is because the controlled perturbations occur along with naturally developing turbulent spots. As a result, the boundary layer statistics are determined from a combination of controlled and natural disturbances.

The mean pressure spectra also show the alteration of the boundary layer at varying Re with the perturber firing (Fig. 8(b)). At a low Re of $6.5 \times 10^6/m$, a large second-mode wave is evident near 175 kHz. When the perturber is firing, the amplitude of the instability wave is lower in the spectra. This is because the boundary layer is more turbulent, leading to more broadband pressure fluctuations (mostly evident between 0–100 kHz) and a smaller average second-mode wave peak. There is also additional electronic noise present when the perturber is firing, but the noise does not hide clear difference in the boundary-layer state with the perturber firing. At higher Re, the boundary layer is again more turbulent with the perturber firing, and the frequency content of the pressure fluctuations is again more evenly distributed across broadband frequencies.

In addition to characterizing the statistical effect of the perturber firing, various turbulent spot growth parameters were also estimated from the controlled disturbances. Even though these parameters do not directly relate to the fluid-structure interactions discussed here, they are important for modeling the fluid dynamics of the problem as discussed in Ref. 2. The typical average pressure disturbance created by the spot can be readily obtained from the ensemble averages. Fig. 7(c) shows that the pressure within the spot is near 1.1 p_e. Downstream of the spot, there is a lower pressure 'calmed region' with a pressure near 0.95 p_e. The presence of the calmed region was observed in previous measurements at Mach 6, however, the average pressures within the spot that are observed here are lower than previously obtained at Mach 6.[1]

The convection velocity of the disturbances was also estimated from the data. This is difficult to do

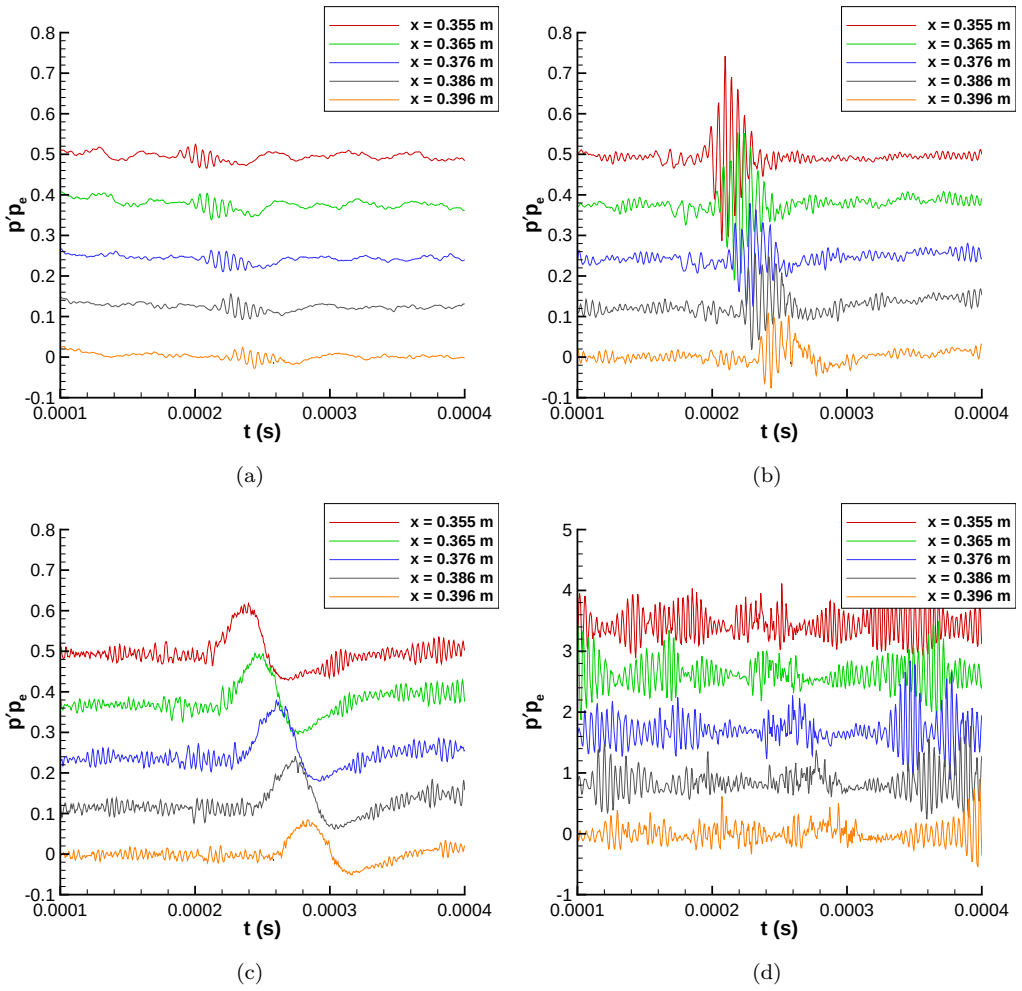

Figure 7. Controlled disturbances along the axial insert, blunt nosetip. Individual traces are offset from each other to show the growth and convection of the disturbances between measurement locations. (a) Ensemble average, $Re = 4.1 \times 10^6/m$; (b) Ensemble average, $Re = 8.4 \times 10^6/m$; (c) Ensemble average, $Re = 14.5 \times 10^6/m$; (d) Individual sample, $Re = 14.5 \times 10^6/m$.

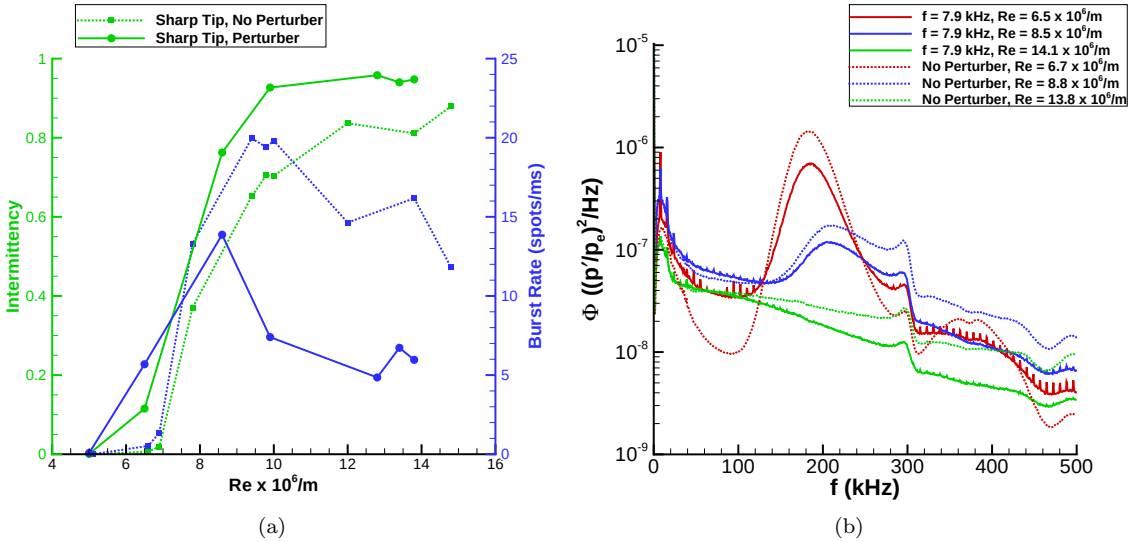

Figure 8. Boundary-layer measurements at x = 0.422 mm, with and without controlled perturbations at 7.9 kHz, sharp nosetip (a) Intermittency and turbulent burst rate computed from PCB132 measurements; (b) Pressure spectra computed from PCB132 measurements.

because of the presence of naturally occurring disturbances that are mixed in with the controlled disturbances. However, best estimates were made from individual disturbances over a range of Re and averaged to give typical convection velocities. The average leading edge velocity was $0.91 \pm 0.07 U_e$ and the average trailing edge velocity was $0.71 \pm 0.07 U_e$. This is in line with typical results at other hypersonic conditions.[2] An attempt to characterize the spanwise spreading angle was also completed. However, the disturbances typically covered the entire spanwise array of sensors and were surrounded by large natural disturbances. This prevented a reliable estimate of the spreading angle from being made.

III.B. Panel Response to Naturally Developed Boundary Layers

The thin-panel cone was first subjected to naturally developing boundary layers. The response of various panel configurations to a fully turbulent boundary layer is shown in Fig. 9. The dominant mode frequencies predicted by the hammer test are shown in each direction with dashed lines. The hammer test predicts many of the dominant frequencies in the spectra. In the axial direction, the two-lobe panel mode P_x can be clearly seen for the various configurations in Fig. 9(a). The mass mode M_x also shows up for the panel configurations with the tungsten mass, though the frequency does not perfectly match. In the spanwise direction, the two-lobe panel mode P_y can be seen (Fig. 9(b)). Once again, the mass mode M_y also shows up, though its frequency is again not perfectly matched. Finally, in the vertical direction, the three-lobe panel mode P_z shows up very clearly (Fig. 9(c)). The frequency shift of this mode with panel configuration is also well predicted by the hammer test. It should be noted that the triaxial accelerometer, G1, used for the measurements in Figs. 9(a) – 9(c) can only characterize frequency content to about 5–8 kHz, so there is attenuation of the higher frequency data shown.

For measurements on the panel itself, the G5 sensor was used and can resolve frequencies above 10 kHz. Fig. 9(d) shows the vertical vibration results. The 3-lobe panel mode P_z is again clearly seen, and the frequency shift of this mode for each configuration is predicted well by the hammer test. Other panel modes, even those dominant in the axial and spanwise direction such as P_x and P_y, show up at this measurement location because the mode shapes do have some displacement associated with the vertical direction. Other high frequency peaks also appear in the spectra (P_{c1}, P_{c2}, and P_{c3}) and are associated with complex panel mode shapes. These shapes were identified by the hammer test, though its frequency response is limited to about 10 kHz, and there is uncertainty in characterizing shapes above about 6 kHz.

Fig. 10 shows the response of the carbon-composite panel across a range of Reynolds numbers. This configuration is used for the remainder of the discussion as similar trends were observed with other panel configurations. The acceleration is normalized by the edge dynamic pressure q_e to allow data acquired at different Re to be compared. The black curve represents a high Reynolds number case near $14.8 \times 10^6/m$ where the boundary layer is mostly turbulent. This is clearly shown in the spectra of pressure sensors upstream and downstream of the panel (Fig. 11). This case exhibits the lowest excitation levels for both accelerations on the mass (G1) and the vertical panel response (G5). Lower Reynolds numbers between 6.6 and $9.8 \times 10^6/m$ correspond to transitional flow over the panel and show elevated responses. Interestingly, the low structural natural frequencies of the panel show little variation with Re. Instead, most of the variation of the panel response with Re is for higher frequency content above 5 kHz. The reason for this high frequency variation will be explored in more detail in the following section.

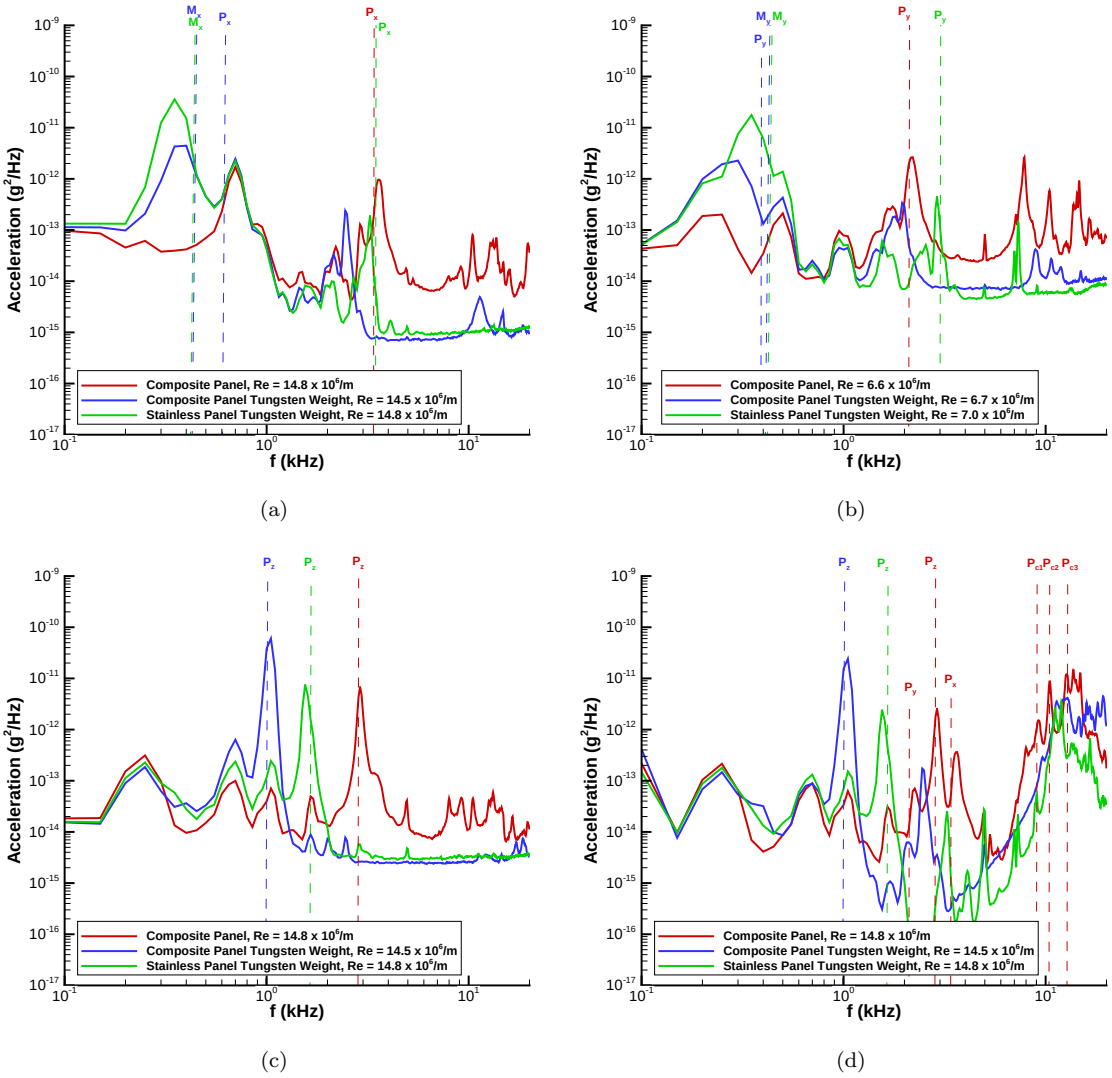

Figure 9. Panel response to a turbulent boundary layer at Mach 8 (a) G1, axial; (b) G1, spanwise; (c) G1, vertical; (d) G5.

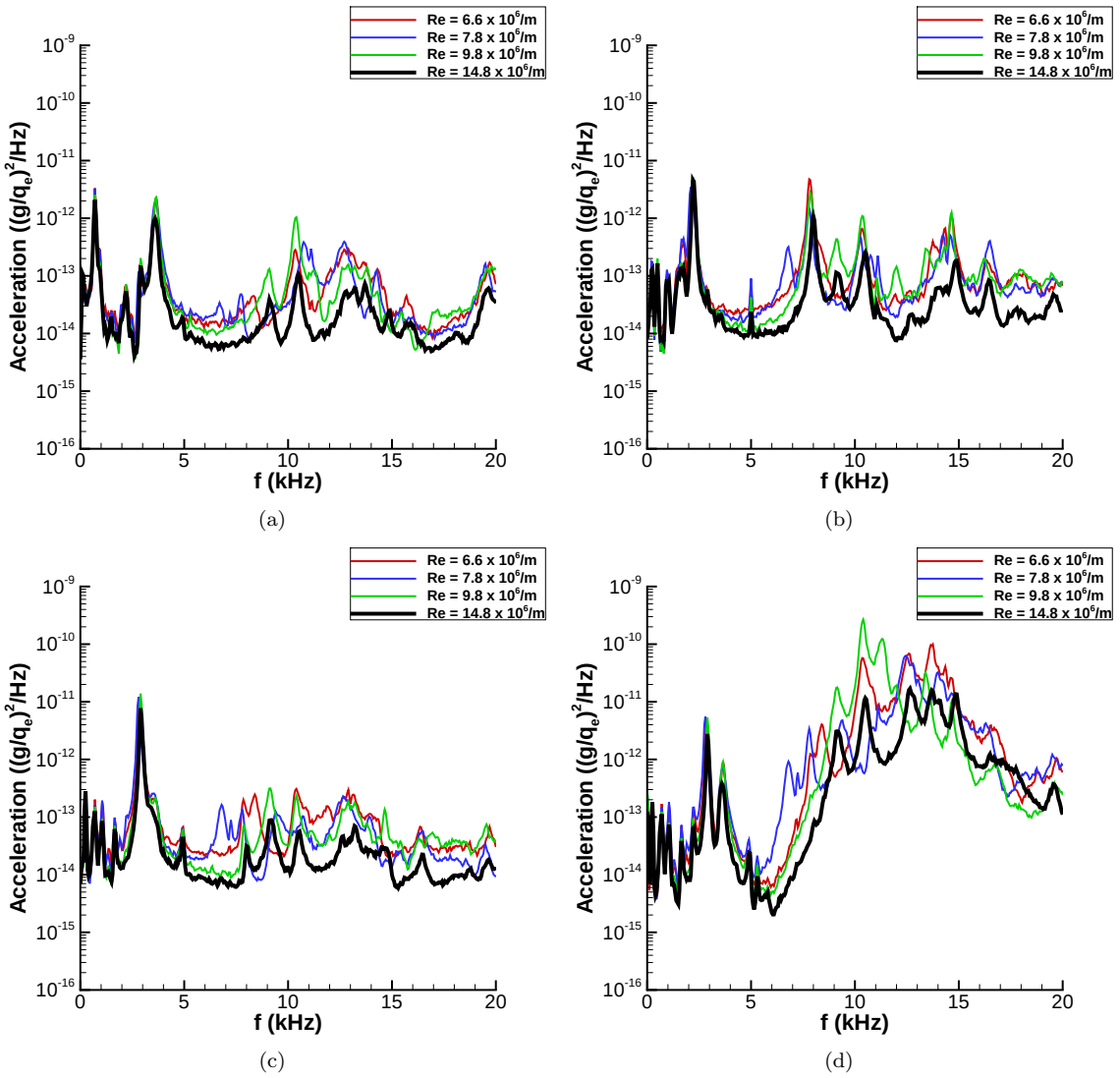

Figure 10. Carbon composite panel response at varying Re, sharp nosetip (a) G1, axial; (b) G1, spanwise; (c) G1, vertical; (d) G5.

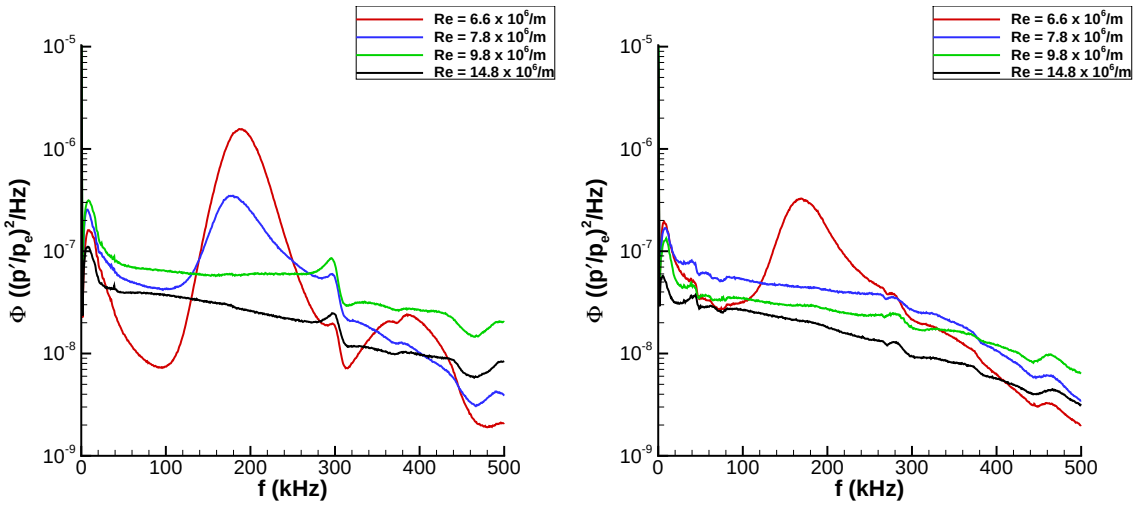

Figure 11. PCB132 pressure-fluctuation power spectra, sharp nosetip (a) x = 0.422 m, upstream of panel; (b) x = 0.497 m, downstream of panel.

III.C. Panel Response to Controlled Perturbations

Panel accelerations were also measured with the perturber firing at various frequencies matching the structural natural modes of the panel. It was initially hypothesized that targeting the dominant panel modes such as P_z would lead to elevated vibrational responses at those frequencies. However, clear changes in the response of the panel at the targeted structural mode frequencies were never observed, regardless of the panel material or attached weight. This was true no matter which specific natural mode of the panel was targeted, whether it was 300 Hz or 7.9 kHz. However, a clear distinction between the transitional vibration response of the panel was observed over a broad frequency range primarily above 5 kHz when the perturber was fired at a high repetition rates above about 4 kHz.

Fig. 12 shows an example of this result for the carbon-composite panel with and without the perturber firing at 7.9 kHz. At low Reynolds numbers near $5.4 \times 10^6/m$, similar results are obtained with and without the perturber (Fig. 12(a)). At a slightly higher Reynolds number near $6.5 \times 10^6/m$, some frequencies, especially near 10 kHz, show elevated responses, while others are lower (Fig. 12(b)). Finally at high Reynolds numbers, the perturber actually lowers the vibration levels over a broad frequency range between 5 and 20 kHz (Figs. 12(c) and 12(d)).

The state of the boundary layer downstream of the panel for these cases is shown in Fig. 13(a). At the lowest Re of $5.4 \times 10^6/m$, the flow is still laminar and dominated by second-mode waves. A large instability peak is observed near 175 kHz, along with a nonlinear harmonic. At Re of $6.5 \times 10^6/m$, the flow is intermittent over the panel. The pressure spectra still show evidence of a second-mode peak, but there are also elevated broadband fluctuations corresponding to intermittent turbulent flow.[3,14] This is because the flow is alternating between second-mode waves and turbulence. At higher Re, the flow is mostly turbulent, as demonstrated by the broadband pressure spectra without evidence of a second-mode instability peak. Although the boundary-layer state is being measured by PCB132 sensors that measure high frequency fluctuations above 11 kHz, they give a clear understanding of the dynamics in the boundary layer. Lower-frequency pressure fluctuations typically measured by Kulite pressure sensors do not clearly show the passage of turbulent spots in the boundary layer and can be easily contaminated by tunnel noise which is highest at low frequencies.[14]

Because the elevated vibrational response occurs when there is intermittent flow over the panel, the transition statistics were again computed for the pressure measurements near the panel. Fig. 13(b) shows the computed statistics downstream of the panel at x = 0.497 m, over a range of Re. At a low Re near $5.0 \times 10^6/m$ the boundary layer is laminar; second-mode waves are present but not turbulent spots, giving a turbulent spot intermittency near zero. At a higher Re of $6.5 \times 10^6/m$, the boundary layer is intermittent when the perturber is firing (near 0.25 at the panel rear). This corresponds to a burst rate near 10 spots/ms at the panel rear. The rate seems to correspond to the elevated panel vibrational response at 10 kHz. It

is expected that the driving panel frequency would be distributed around 10 kHz if the burst rate is 10 spots/ms, since the spots would occur with some non-uniform spacing between them. Note that this burst rate is not same as the rate of the perturber firing, because the controlled disturbances are occurring at the same time as natural turbulent spots. The effective burst rate therefore depends on both the perturber firing frequency and the natural turbulent burst rate and must be computed from the PCB132 sensors upstream and downstream of the panel. At higher Re of 8.8 and $14.5 \times 10^6/m$, when the perturber is on, the intermittency is higher and the burst rate is lower in comparison to measurements without perturbations. This causes a lower vibration response of the panel because the flow is more turbulent (less switching between laminar and turbulent flow when the perturber is firing).

These results suggest that the intermittent flow is driving the panel response at these high frequencies. If this is true, than the same trend should be demonstrated at a slightly higher Re for a blunt nosetip, since the nosetip bluntness delays transition on the cone.[13] This same trend does indeed occur. Fig. 14(a) shows the acceleration response of the panel over a range of Re with the blunt nosetip. Elevated vibrational responses are seen near 12 kHz at an Re of $8.9 \times 10^6/m$ where intermittent flow is observed. The turbulent burst frequencies are computed to be near 12 spots/ms at the end of the panel (Fig. 14(b)), which would again be expected to force the panel with some frequency distribution centered around 12 kHz. At higher Re where the flow is more turbulent, a reduced response of the panel is again observed with the perturber firing. Finally, the same trend should also occur for a natural transition case on the sharp nosetip, without the perturber firing. This is because, as discussed in Section III.A, the perturber creates a higher level of intermittency and a lower overall burst rate in comparison to the natural transition case. Once again, elevated vibrations near 9–11 kHz do occur at a higher Re near 8.8×10^6/m (Fig. 15(a)).

Together, these experiments support the hypothesis that intermittent flow is driving the panel response at these high frequencies. However, a more definitive way to correlate the panel response to the flow excitation is still needed. This is difficult to do from the present data because the perturber is not the driver for the boundary-layer state at Mach 8. The perturber modifies the flow (advances transition by increasing the boundary-layer intermittency and decreasing the turbulent burst rate), but the flow is still primarily driven by the natural boundary-layer development.

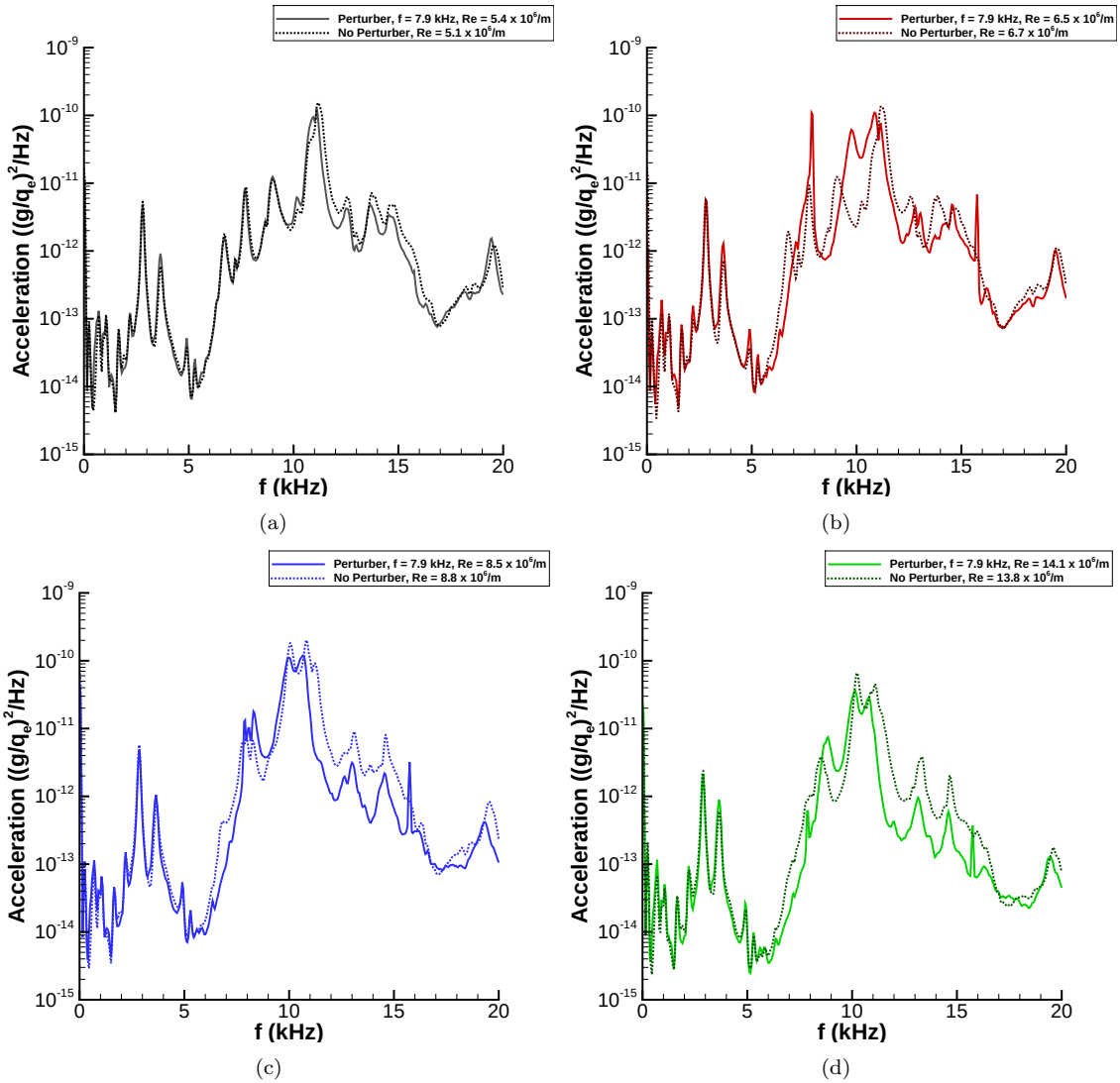

Figure 12. Composite panel response at G5 with and without the controlled perturbation at 7.9 kHz, sharp nosetip (a) Re **near** $5.4 \times 10^6/m$**; (b)** Re **near** $6.5 \times 10^6/m$**; (c)** Re **near** $8.5 \times 10^6/m$**; (d)** Re **near** $14.1 \times 10^6/m$**.**

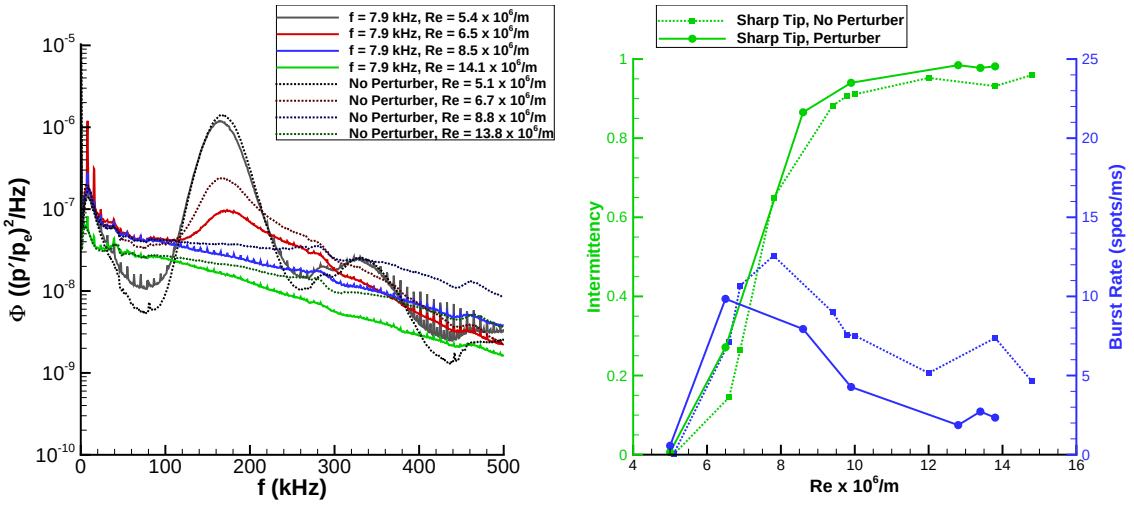

(a) (b)

Figure 13. Boundary-layer measurements downstream of the panel at x = 0.497 m, with and without controlled perturbations at 7.9 kHz, sharp nosetip (a) Pressure spectra computed from PCB132 measurements; (b) Intermittency and turbulent burst rate computed from PCB132 measurements.

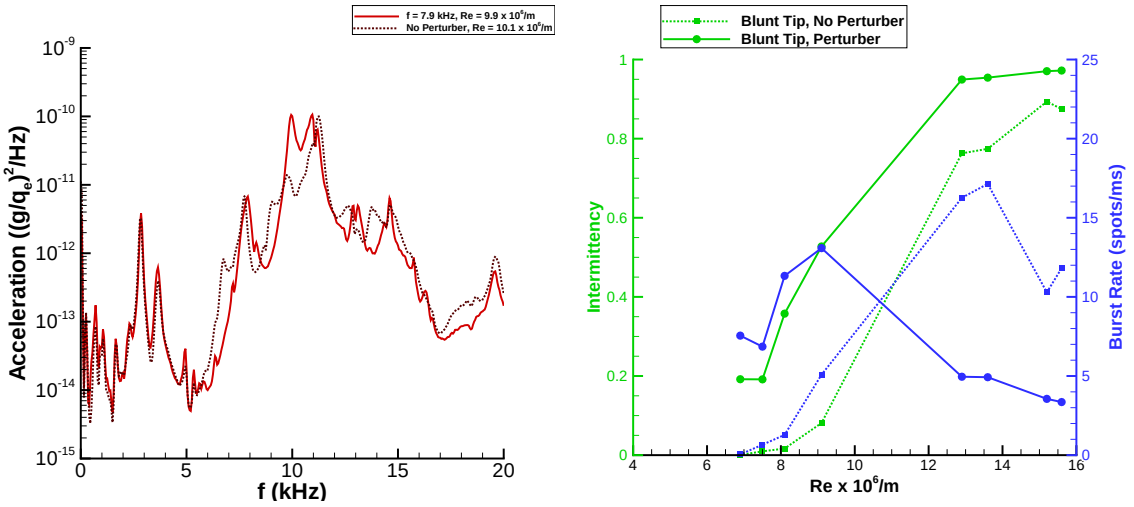

(a) (b)

Figure 14. Carbon-composite panel measurements, perturbation at 7.9 kHz, blunt nosetip (a) Vibration response of panel; (b) Intermittency and burst rate computed from PCB132 measurements downstream of panel at x = 0.497 m.

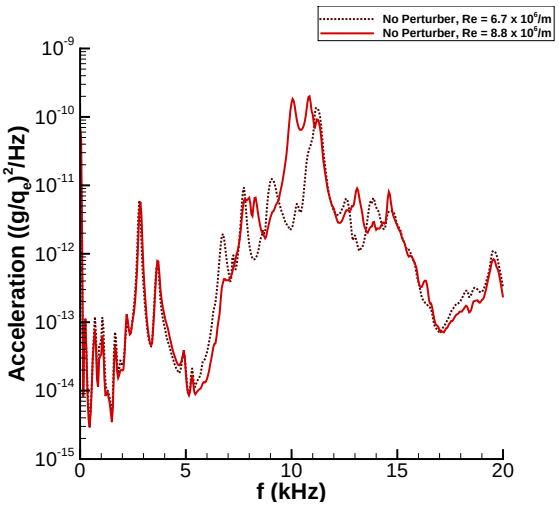

(a)

Figure 15. Elevated transitional vibrations under natural boundary-layer transition, sharp nosetip.

IV. Concluding Remarks

A novel experiment has been developed to study high speed fluid-structure interactions on a slender cone in Sandia's Mach 8 Hypersonic Wind Tunnel. A thin panel was integrated into the rear of a 7° half-angle cone and then exposed to naturally developing boundary layers. The response of the panel to boundary-layer flow excitation was measured with internal accelerometers. Elevated panel responses were observed during boundary-layer transition, and a lower response was seen for turbulent boundary layers. The elevated response occurred primarily at high frequencies near 9–12 kHz. This driving frequency appeared to be related to the turbulent burst rate on the cone during boundary-layer transition.

The panel response was then measured with and without additional controlled perturbations. Similar vibration levels were measured for freestream conditions where the flow remained laminar both with and without the additional controlled perturbations. For freestream conditions corresponding to transitional flow over the panel, an elevated response was measured when the perturber was turned on. The frequency of the elevated vibration response again corresponded to the turbulent burst rate over the panel, which was caused by a combination of controlled and natural turbulent spots. At even higher freestream Reynolds numbers, the controlled perturbations created a lower vibration response of the panel. This is likely because the perturber created more turbulent flow (higher intermittency and a lower burst rate) than the natural flow without the perturber. This lower burst rate led to a lower vibrational response of the panel.

Further investigation of the potential correlation of the turbulent burst rate and transitional panel vibration response is needed. Future tests are planned at Mach 5 where it is more likely that the perturber will be a driver for the boundary-layer state instead of only modifying the naturally developing boundary layers as occurred at Mach 8. The tunnel noise is much lower at Mach 5, and the dominance of second-mode waves is smaller as discussed in Ref. 14. Therefore, it may be easier to initiate controlled disturbances on the cone which could drive the boundary-layer response. Potential experiments are also planned in the Boeing/AFOSR Mach-6 Quiet Tunnel at Purdue University. The panel can be exposed to controlled perturbations under both noisy and quiet flow. Under quiet flow, the perturber should again be the only driver for panel vibrations, instead of competing against the natural transition process.

Acknowledgments

Since this work forms a new effort in high-speed fluid-structure interactions, it benefited from conversations with and contributions from many individuals. Scott Stanfield provided advice on the conceptual design of the new glow perturber electronics, and Evan Mayerhoff at High Voltage Connection built and designed the final perturber electronics. Mikhail Mesh provided design advice and was involved in many helpful discussions for the panel design. Tom Grasser spent many hours refining the model drawings. David

Calkins and Bill Miller built the composite panel. Paul Farias modified the as-built cone and panel hardware to smoothly integrate all the pieces.

References

[1]Casper, K., *Pressure Fluctuations Beneath Turbulent Spots and Instability Wave Packets in a Hypersonic Boundary Layer*, Ph.D. Thesis, Purdue University School of Aeronautics & Astronautics, August 2012.

[2]Casper, K., Beresh, S., and Schneider, S., "Pressure fluctuations beneath instability wavepackets and turbulent spots in a hypersonic boundary layer," *Journal of Fluid Mechanics*, Vol. 756, 2014, pp. 1058–1091.

[3]Casper, K., Beresh, S., Henfling, J. F., Spillers, R. W., Pruett, B. O. M., and Schneider, S., "Hypersonic Wind-Tunnel Measurements of Boundary-Layer Transition on a Slender Cone," *Accepted for Publication in AIAA Journal*, To Appear 2016.

[4]Maestrello, L. and Linden, T. L. J., "Measurements of the Response of a Panel Excited by Shock Boundary-Layer Interaction," *Journal of Sound and Vibration*, Vol. 16, No. 3, 1971, pp. 385–391.

[5]Willems, S., Gülhan, A., and Esser, B., "Shock Induced Fluid-Structure Interaction on a Flexible Wall in Supersonic Turbulent Flow," *Progress in Flight Physics*, Vol. 285–308, 2013.

[6]Spottswood, S. M., Beberniss, T. J., and Eason, T. G., "Structural Response Prediction: Full-field, Dynamic Pressure and Displacement Measurements of a Panel Excited by Shock Boundary-Layer Interaction," Interim report AFRL-RQ-WP-TP-2015-0046, Air Force Research Laboratory, February 2015.

[7]Gogulapati, A., Deshmukh, R., McNamara, J., Vyas, V., Wang, X., Mignolet, M., Beberniss, T., Spottswood, S., and Eason, T., "Response of a Panel to Shock Impingement; Modeling and Comparison with Experiments," AIAA Paper 2014-0148, January 2014.

[8]Gogulapati, A., Deshmukh, R., McNamara, J., Vyas, V., Wang, X., Mignolet, M., Beberniss, T., Spottswood, S., and Eason, T., "Response of a Panel to Shock Impingement; Modeling and Comparison with Experiments Part 2," AIAA Paper 2015-0685, January 2015.

[9]Wilby, J. F., "The Response of Simple Panels to Turbulent Boundary Layer Excitation," Technical Report AFFDL-TR-67-70, Air Force Flight Dynamics Laboratory, October 1967.

[10]Coe, C. F. and Chyu, W. J., "Pressure-Fluctuationl Inputs and Response of Panels Underlying Attached and Separated Supersonic Turbulent Boundary Layers," *AGARD Symposium on Acoustic Fatigue*, May 1973, pp. 5–1 – 5–20.

[11]Ostoich, C. M., Bodony, D. J., and Geubelle, P. H., "Interaction of a Mach 2.25 Turbulent Boundary Layer with a Fluttering Panel using Direct Numerical Simulation," *Physics of Fluids*, Vol. 25, No. 110806, 2013, pp. 1–27.

[12]Blackman, D. R., Clark, D. M., McNulty, G. J., and Wilby, J. F., "Boundary Layer Pressure Fluctuations and Structural Response," Technical Report AFFDL-TR-67-97, Air Force Flight Dynamics Laboratory, October 1967.

[13]Casper, K. M., *Hypersonic Wind-Tunnel Measurements of Boundary-Layer Pressure Fluctuations*, Master's Thesis, Purdue University, School of Aeronautics & Astronautics, August 2009.

[14]Casper, K., Beresh, S., Henfling, J. F., Spillers, R. W., and Pruett, B. O. M., "Toward Transition Statistics Measured on a 7-Degree Hypersonic Cone for Turbulent Spot Modeling," AIAA Paper 2014-0427, January 2014.

[15]Ladoon, D. W., *Wave Packets Generated by a Surface Glow Discharge on a Cone at Mach 4*, Ph.D. Thesis, Purdue University, School of Aeronautics & Astronautics, December 1998.